ACS OMEGA

http://pubs.acs.org/journal/acsodf

Review

A Critical Review on the Development of Optical Sensors for the Determination of Heavy Metals in Water Samples. The Case of Mercury(II) Ion

Graciela M. Escandar* and Alejandro C. Olivieri*

Cite This: *ACS Omega* 2022, 7, 39574−39585

Read Online

ACCESS | Metrics & More | Article Recommendations

ABSTRACT: Recent publications are reviewed concerning the development of sensors for the determination of mercury in drinking water, based on spectroscopic methodologies. A critical analysis is made of the specific details and figures of merit of the developed protocols. Special emphasis is directed to the validation and applicability to real samples in the usual concentration range of mercury, considering the maximum allowed limits in drinking water established by international regulations. It was found that while most publications describe in detail the synthesis, structure, and physicochemical properties of the sensing phases, they do not follow the state of the art in the analytical developments. Recommendations are provided regarding the proper method development and validation, including the setting of the calibration concentration range, the correct estimation of the limits of detection and quantitation, the concentration levels to be set for producing spiked water samples, the number of real samples for adequate validation, the comparison of the developed method with a reference technique, and other analytical features which should be followed.

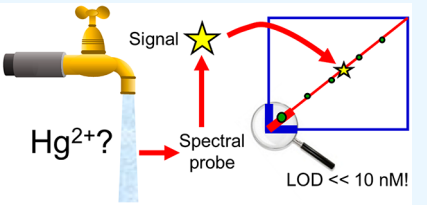

1. INTRODUCTION

Safe and readily available water is important for public health.[1] Drinking water may contain small amounts of heavy metals, some of which are known to be essential for human health. However, an excess of essential metal ions, or even small quantities of other ions may have a serious negative impact.[2] The presence of heavy metals in water is due to several reasons: (1) the release into the environment by natural causes; (2) anthropogenic activities, such as industrial activities generating wastes (electroplating, metal smelting and chemical industries); or (3) poorly treated wastewaters.[3]

There is a growing number of publications devoted to the development of new spectroscopic platforms for the determination of inorganic ions in samples such as drinking and natural waters, foodstuff, etc., which are of high importance for consumer safety. The methods are based on either absorptimetric or emissive probes, which are developed in such a way that they are highly selective and proposed to be sufficiently sensitive to the presence of specific metal ions in the studied samples. The advantages of the proposed sensors include simplicity, low cost, and speed.[4] Typically, the concentrations to be measured in the latter samples are small, requiring limits of detection which should be compatible with the maximum levels set by international regulating agencies. Therefore, efforts are directed to maximize the sensitivity of the analysis, by incorporating a series of clever approaches in the new developments.

Due to the large number of papers published in recent years on the subject, the present report is concerned with a specific case: the determination of mercury in drinking water. This analyte was selected because of the challenges in measuring very low concentrations due to its toxicity. However, most of the considerations regarding chemical analysis at low concentrations also apply to other heavy metal ions, anions and organic pollutants in environmental samples, foodstuff, etc.

The sources of mercury in water include the erosion of natural deposits, the discharge from refineries and factories, and the runoff from landfills and croplands. For metal ions and other contaminants, the US Environmental Protection Agency (EPA) sets two limits:[5] (1) the Maximum Contaminant Level Goal (MCLG), which is the level of a contaminant in drinking water below which there is no known or expected risk to health; and (2) the Maximum Contaminant Level (MCL), which is the highest level of a contaminant that is allowed in drinking water and is an enforceable standard. MCLs are set as close to MCLGs as feasible using the best available treatment technology and taking cost into consideration. In the case of mercury, the MCLG and MCL are both 2 μg L^{-1} (2 ppb, 10 nM).[5] Below this level of mercury in drinking water, there is no known or expected risk to health. Otherwise, serious problems may arise, the main of which is kidney damage.[6]

Received: August 14, 2022
Accepted: October 14, 2022
Published: October 27, 2022

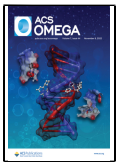

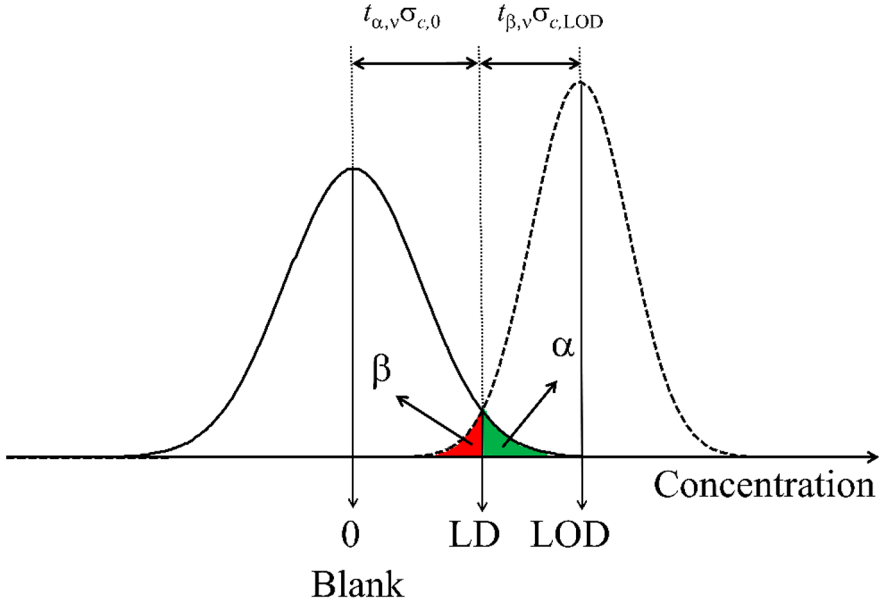

Figure 1. Scheme illustrating the modern IUPAC definition of the limits of decision (LD) and detection (LOD). Gaussian lines are shown centered at the blank and at the LOD level. The LD decides whether the analyte is detected or not with a rate α of false positives (green shaded area), whereas the LOD implies detection with a rate α of false positives and a rate β of false negatives (red shaded area). Adapted with permission from ref 8. Copyright 2015 Elsevier.

The analytical method recommended by the EPA for the determination of mercury in drinking water is cold vapor atomic absorption spectrometry.[7] The concentration range of the method is 0.2−10 μg L^{-1} (i.e., the lowest calibration concentration is well below the MCL for Hg in this type of samples). It is recommended to estimate the method detection limit (MDL) as 3 times the standard deviation of 7 replicates of a sample prepared to contain twice the concentration corresponding to a rough estimation of the true LOD. However, modern IUPAC recommendations use a different concept for the LOD estimation, which will be discussed below in detail.[8,9]

It is apparent that both the LOD and LOQ must be low enough to detect and measure mercury concentrations at the required levels according to official regulations. If the LOQ of a new method is larger than the MCL, then it should probably be called a method to detect Hg in highly contaminated water samples and may require a substantial preconcentration step for analyzing drinking water. Nevertheless, even if the detection capability of a method is adequate, it should be appropriately validated to be considered reliable. In the present report, we review a number of selected publications on the development of spectroscopic methods for determining Hg in water samples, with emphasis on the requirements to be met for achieving the intended purpose.

2. RECOMMENDATIONS ON FIGURES OF MERIT

Analytical reports should not only describe with particular detail the synthesis, structure, and physicochemical properties of a new chemosensor or probe for specific analytes. The analytical section should be as complete as possible, following the standard guidelines which include the figures of merit, the statistical analysis of the results, and the comparison with those provided by previously published methods. Below we summarize the main figures of merit that should be reported and recommendations for the correct statistical analysis and method comparison.

2.1. Sensitivity. The sensitivity and analytical sensitivity should be reported, preferably including a comparison with the same parameters in previous analytical reports on the same analyte. The sensitivity is defined as the slope of the calibration graph; however, the analytical sensitivity is preferred for method comparison because it is independent of the measured signal.[10,11] The latter is defined as the ratio of the sensitivity and the instrumental noise level and has inverse concentration units.

2.2. Linearity. Most authors still employ the correlation coefficient (R^2) of the calibration line as an indicator of the linear relationship between signal and concentration. IUPAC discourages this practice, recommending the estimation of an F value as the ratio of the residual variance of the calibration line to the variance of the instrumental noise. Comparison should be made with the critical F value, as detailed in a IUPAC report.[12] Other relevant discussions can be found in the literature.[13]

2.3. Limits of Detection and Quantification. The definition of the LOD has been evolving with time, from the old concept based on three times the standard deviation for the blank, to the modern view considering both Type I and Type II errors, also called α and β, or false positives and false negatives.[7,14,15] Furthermore, error propagation should consider the uncertainties in the measurement of the test sample and also those coming from the calibration phase. Specifically, the modern IUPAC recommendation first requires to define the limit of decision (LD), which only considers a risk of false positives (Figure 1, green-shaded area). The limit of detection is then defined as the level for which the risk of false negatives has a probability β, corresponding to the red-shaded area in Figure 1. According to this latter figure, the expression for the LOD is

$$\mathrm{LOD} = t_{\alpha,\nu}\sigma_{c,0} + t_{\beta,\nu}\sigma_{c,\mathrm{LOD}} = \frac{3.3 s_{y/x}}{m}\sqrt{1 + h_0 + \frac{1}{N}} \quad (1)$$

https://doi.org/10.1021/acsomega.2c05215
ACS Omega 2022, 7, 39574−39585

where $t_{\alpha,\nu}$ and $t_{\beta,\nu}$ are student coefficients with $\nu = N - 2$ degrees of freedom and probabilities α and β respectively, N is the number of calibration samples, $\sigma_{c,0}$ and $\sigma_{c,\mathrm{LOD}}$ are the concentration standard errors at the blank and LOD levels, m is the slope of the calibration line, and $s_{y/x}$ is the residual standard deviation. Assuming $\sigma_{c,0} = \sigma_{c,\mathrm{LOD}}$, the 95% confidence level ($\alpha = \beta = 0.05$) and a large number of degrees of freedom, the right-hand side of eq 1 is obtained, where h_0 is the blank leverage value given by

$$h_0 = \frac{\overline{c}_{\mathrm{cal}}^2}{\sum_{i=1}^{N} (c_n - \overline{c}_{\mathrm{cal}})^2} \tag{2}$$

where $\overline{c}_{\mathrm{cal}}$ is the mean calibration concentration and c_n represents the concentration of the analyte in the n^{th} calibration sample.

In some cases, authors refer to the IUPAC definition of the LOD but still use the old definition. The following important remarks by IUPAC should be considered: "It is accordingly recommended that...the approximate detection limit (is) calculated as 3S0. Note that with the recommended minimum number of degrees of freedom, this value is quite uncertain, and may easily be in error by a factor of 2. Where more rigorous estimates are required (e.g., to support decisions on based on detection or otherwise of a material), reference should be made to appropriate guidance (see, e.g., refs 22, 23)." In these latter references the new definitions of the LOD and LOQ are provided.[16,17]

Another relevant issue is the use of the log transformation for coping with nonlinear signal-concentration relationships. However, it is preferable to employ the nonlinear calibration line, estimating the LOD according to a recent procedure, adapted from the IUPAC recommendations for linear calibration lines.[18]

Due to the presence of additional terms in the square root of eq 1 beyond the classical value of 1, the modern LOD definition is stricter (i.e., larger) than the old one. It is important to notice that all the reviewed publications quote the incorrect detection capability based on the abandoned LOD definition. They are consequently lower (perhaps significantly) than the true LOD values.

Even more important than the LOD is perhaps the limit of quantitation (LOQ) defined as

$$\mathrm{LOQ} = \frac{10 s_{y/x}}{m} \sqrt{1 + h_0 + \frac{1}{N}} \tag{3}$$

where the factor 10 sets a relative prediction uncertainty of 10%. The relevance of the LOQ is that the linear range of a developed method for the determination of mercury ranges from the LOQ to the upper concentration limit where the linear signal-concentration relationship holds. To be able to quantitate Hg below the levels set by official agencies, a sufficiently low LOQ is required.

2.4. Significant Figures. It is not uncommon to find reported analytical results with an excessive number of significant figures, which is unreasonable. In general, all results should be reported with a number of significant figures compatible with the associated standard error. In the case of uncertainty measures (standard errors, root-mean-square errors, relative prediction errors) and also in the case of parameters derived from uncertainties (detection limit, quantitation limit), they should be reported with one or at most two significant figures. A good rule of thumb is to use two significant figures when the first one is 1, or when the first is 2 and the second is smaller than 5; in the remaining cases, a single significant figure should be reported.[8]

2.5. Statistical Analysis of the Results. The number of studied samples is usually too small to gather reliable information on the applicability of the method. A new analytical development should include the validation of the protocol with a number of test samples (preferably certified reference materials or real samples, not artificially laboratory-prepared or spiked samples), comparing the determined concentrations of the analyte with those provided by a reference standard technique. The estimated recovered values should be compared with reference values. Statistical tests should be applied to assess whether a recovery is not statistically different than 100%, reporting both the experimental and critical t values. It should be noticed, however, that these tests assume certain conditions that the data should fulfill, such as constant variance.[19,20]

2.6. Comparison of Average Errors. When comparing the average analyte errors estimated by different methods, the conclusions are often drawn on a visual basis. This impression may be false, and an objective statistical technique is required to compare error values, to be able to conclude that one error is significantly smaller than a second one. One interesting alternative is the randomization test described by van der Voet.[21] The latter paper provides an easily implementable computer code in its Appendix.

3. CHEMICAL SENSORS FOR MERCURY IONS

The conventional analytical approaches for Hg(II) analysis include atomic absorption spectroscopy, inductively coupled plasma mass spectrometry, and atomic fluorescence spectrometry. Because these methods are rather complex, expensive, nonportable, and require specialized laboratories, the current scientific efforts are directed to developing efficient chemical sensors as alternatives for the determination of mercury in environmental samples. In general, these sensors display analytical features that make them attractive and useful to be implemented both in the analytical laboratory and in the field. For the present discussion, we have selected and analyzed some reported optical mercury sensors where absorption, fluorescence, and/or surface enhanced Raman scattering are the measured signals.

Most optical sensors for the detection of Hg(II) in aqueous media involve the use of noble metal nanostructures due to their unique physicochemical properties. For example, they have the ability to support surface plasmons which are generated by the coupling between the incident electromagnetic waves and the conduction electrons.[22] In other words, when the electromagnetic radiation of a certain frequency interacts with the metal nanoparticles, their conduction electrons collectively oscillate on a metal/dielectric interface. This resonance is called surface plasmon resonance (SPR) or, more precisely, local SPR (LSPR) because nanoparticles are involved. Gold- and silver nanoparticles, either bare or with functionalized surfaces, are the two most widely used plasmonic nanomaterials, which have demonstrated sensitive LSPR signals used for the selective detection of Hg(II) ion.[22,23] The LSPR spectra can be modified by tailoring the size, the shape (rod, cube, disc, etc.), the structures (shell, cage, tube, etc.), and the environment of the metal nanostructures. The LSPR sensing mechanism can be produced through the aggregation of the nanoparticles or by

https://doi.org/10.1021/acsomega.2c05215
ACS Omega 2022, 7, 39574−39585

changes in their refractive index.[24] The aggregation of nanoparticles, generally functionalized with oligonucleotides, oligopeptides, or chemical functional molecules, is promoted by the Hg(II) ion through its affinity with specific functional groups of the surface, producing a shift of the LSPR band as a result of the strong coupling between the localized SPRs of the nanostructures. On the other hand, refractive index sensors are based on the LSPR peak shift due to the variation in the local refractive index induced by a mercury amalgamation on the nanoparticle surface. In this case, the Hg(II) ion is reduced with an adequate reagent ($NaBH_4$, citrate, etc.) and the generated Hg(0) is strongly bonded onto the surface of either Au- or Ag- based nanomaterials to form an amalgam, shifting the LSPR spectrum of the nanoparticles to shorter wavelengths.[25]

An alternative colorimetric assay is based on the inhibition of the peroxidase-like activity of noble metal nanostructures by the Hg(II) ion. The reaction between the chromogenic substrate 3,3′,5,5′-tetramethylbenzidine (TMB) and H_2O_2 is generally chosen for these probes. When the catalytic activity of the nanostructure decreases due to the presence of the Hg(II) ion, the concentration of the oxidation product decreases, leading to a color change of the system.[26,27]

In other cases, the presence of mercuric ion produces the opposite effect to that described above. For example, the formation of either the stable thymine complex (T-Hg^{2+}-T) or amalgams with noble metals, can reverse the inhibitory effect that certain molecules or nanoparticles have on the oxidase mimetic activity of specific nanostructures. In the presence of Hg(II) ions, the oxidase-like activity of the indicated nanostructures is restored and the concentration of the oxidation product increases.[28,29]

Fluorescent sensors are constituted by nanomaterial-bound fluorescent units (the fluorophores). When the cation binds to the sensor, the fluorophore photophysical properties change due to different processes (photoinduced electron transfer or charge transfer, energy transfer, excimer formation, etc.), leading to either a fluorescence intensity enhancement or to a quenching effect.[23]

Another class of optical sensors for Hg(II) ion resort to surface enhanced Raman spectroscopy (SERS), combining laser spectroscopy with the optical properties of nanosized noble metal structures, resulting in significantly increased Raman signals.[30] The SERS methods for the detection of Hg^{2+} are based on either the specific interaction between the ion and Raman active molecules exhibiting a strong and specific SERS spectrum (reporters) or the formation of the T-Hg^{2+}-T complex. The detection of the Hg(II) ion is achieved by enhancing or turning off the SERS signals of the Raman reporters. The DNA-based T-Hg^{2+}-T system relies on the coordination chemistry of the metal ion with the nucleotide and the formation of nanoparticles aggregates with the concomitant changes in the SERS intensity.

Some research groups have proposed the mercury determination by simultaneously measuring two types of signals with the same sensor, one detection mode generally being superior to the other. However, in some of these dual methods one of the two types of signal results in an unfeasible LOD for the determination of low levels of Hg(II) ion. Thus, it would be more correct to characterize the method with the signal that allows achieving the analytical purpose rather than as a dual one.

4. REVIEW ON MERCURY SENSOR REPORTS

As indicated above, numerous scientific articles report the determination of the mercury(II) ion in water samples. For the sake of brevity, we have randomly selected a number of publications on optical mercury sensors. The information from the literature search was compiled in Tables 1−4 following an increasing order of publication year and were organized according to the measured spectroscopic signals, as detailed in Section 3. Thus, whereas Tables 1, 2 and 3 describe sensors based on absorption, fluorescence, and SERS signals, respectively, Table 4 includes sensors displaying two different types of signals.

The first and second columns of these tables show the operational basis of the sensors and the relationship between the measured signal and the mercury concentration. In the next column, the analytical efficiency of each of the proposed methods is briefly mentioned, with an emphasis on both the linear range and the attained limit of detection. Regarding the values of these latter parameters in the tables, it is important to point out that none of them was calculated using the modern IUPAC definition (see above). Nevertheless, to assess and compare the detection capabilities of the sensors, the reported LODs were used in our discussion. To facilitate the comparison among the different works, the concentration units were unified to micrograms per liter (parts-per-billion).

The tables also include the type of studied water sample, the applied pretreatment (if any), the added mercury concentrations to the spiked samples and/or the original values found in real samples without addition of the analyte. Since in these latter samples the Hg(II) ion content is unknown, it is mandatory to compare the obtained results with those provided by a reference method.

From the 42 selected methods shown in the tables, only two of them meet the correct analytical standards for the validation protocol in real samples.[28,31] Qi et al.[28] developed a colorimetric mercury sensor blocking with the Hg(II) ion the inhibition produced by oligonucleotides on the peroxidase-mimicking catalytic activity of graphene oxide/AuNPs in the oxidation of 3,3′,5,5′-tetramethylbenzidine (TMB) by H_2O_2. Under the optimized conditions, a calibration line was built with the absorbance at a proper wavelength as a function of the mercury ion concentration. Seven replicate calibration samples containing Hg(II) concentrations from 1.04 $\mu g\ L^{-1}$ to 24 $\mu g\ L^{-1}$ were employed. Although the limit of detection (LOD = 0.076 $\mu g\ L^{-1}$) was calculated with the old LOD concept, the value was below the US EPA maximum level in drinking water of 2 $\mu g\ L^{-1}$. The method was successfully applied in both spiked and real samples without externally added analyte, and the estimated concentrations were compared with those provided by a reference method.

On the other hand, Zheng et al. quantified mercury in tap, pond, and river waters using a fluorescence sensor.[31] The latter was based on the capability of the Hg (II) ion to remove the quenching effect AuNPs modified with thioglycolic acid on the fluorescence of rhodamine B by disrupting the absorption of the dye molecules on the surface of the nanoparticles. The calibration was performed under optimal experimental conditions, measuring the fluorescence intensity at the emission maximum as a function of analyte concentration, ranging from 0.2 to 6.2 $\mu g\ L^{-1}$. The LOD calculated as the ratio between three times the standard deviation of the blank signal, and the slope of the calibration line was 0.08 $\mu g\ L^{-1}$.

https://doi.org/10.1021/acsomega.2c05215
ACS Omega 2022, 7, 39574−39585

Table 1. Hg(II) Ion Determination in Water Samples Using Absorptimetric Signals

probe/sensor fundamentals	calibration graph[a]	LR ($\mu g\ L^{-1}$)	LOD ($\mu g\ L^{-1}$)	samples/evaluated $C_{Hg(II)}$	ref
Hg interacts with AuNRs in a $NaBH_4$ solution. $C_{Hg(II)}$ is directly related with the blue shift of the maximum absorption wavelength of the longitudinal mode band of AuNRs. LOD after amalgam formation is ca. parts-per-trillions.	$(\Delta\lambda_{fd})^b$ vs $C_{Hg(II)}$	1.98×10^{-6}–0.031	$(6.6 \times 10^{-7})^c$	One tap water sample (multiple standard addition method). Original Hg(II) ion concentration: 1.67×10^{-3} $\mu g\ L^{-1}$. No sample separation or preconcentration required.	33
NPs suspension of Hg(II) ion-dithizone complex is filtered and quantified on the surface of a WX mixed cellulose membrane through UV–visible DRS. The colored Hg–dithizone complex is directly measured on the surface of membrane	A_{485} vs $C_{Hg(II)}$	0.2–4.0	0.12[c]	Tap and river waters filtered through 0.22 μm membranes were treated with $KMnO_4$ and $K_2S_2O_8$. Three samples of each water were spiked with 0.5; 1.5 and 3 $\mu g\ L^{-1}$ Hg(II) ion. AFS was applied.	34
Hg(II) ion induces both deprotection and morphology transition of 1-dodecanethiol-capped AgNPRs in the presence of iodide, producing a color change of the system. The $\Delta\lambda$ of the SPR band is used for quantifying Hg(II) ion.	$\Delta\lambda$ vs $C_{Hg(II)}$	2–100	0.66[c]	Tap, drinking, and lake waters were filtered through 0.22 μm membranes. Three samples of each water were spiked with 0; 40 and 80 $\mu g\ L^{-1}$ Hg(II) ion.	35
Hg(II) ions are reduced by Ag-AuNPs electrodeposited on indium tin oxide film coated glass. The deposition/amalgamation leads to a blue shift of the SPR peak.	$\Delta\lambda$ vs $C_{Hg(II)}$	0.05–500	0.02[c]	Hg(II) levels found in tap (0.61 $\mu g\ L^{-1}$) and lake (0.87 $\mu g\ L^{-1}$) waters were close to CVAAS (0.67 and 0.83 $\mu g\ L^{-1}$, respectively). No sample separation or preconcentration required.	24
Aggregation of citrate-stabilized AuNPs in the presence of Hg(II) ion and lysine (positively charged) induces a color change of the system. Lysine is used as an aggregation promoter of Hg(II) ion-covered AuNPs.	A_{725}/A_{525} vs $C_{Hg(II)}$	0.2–200	0.58[c] (dw), 0.78[c] (tw)	Two tap water samples were spiked with 1 $\mu g\ L^{-1}$ Hg(II) ion.	36
Hg(II) interacts with an aqueous dispersion of cysteamine stabilized AgNPs, forming a Ag–Hg nanoalloy, and the system changes from yellow to colorless	A_{402} vs $C_{Hg(II)}$	0.055–2.7	0.055	Lake, tap and packaged drinking waters were filtered through Whatman-1 paper. One sample of each water was spiked with 1 $\mu g\ L^{-1}$ Hg(II) ion.	37
AuNPs/Hg amalgam catalyzes the reduction of 4-NP by $NaBH_4$. As $C_{Hg(II)}$ increases, the reduction time decreases. When Hg deposition reaches saturation, AuNPs aggregation occurs, the reduction time increases, and the color changes.	CCT_{400} vs log $C_{Hg(II)}$	0.2–20 (CCT ↓) 20–160 (CCT ↑)	0.29[c]	One tap water spiked with 0.2; 1; 2; 10; 20; 60; 100; 160 and 200 $\mu g\ L^{-1}$ Hg(II) (standard addition method). ICP-MS was also applied.	38
Hg(II) ion increases the absorbance of self-doped copper-deficient $Cu_{2-x}Se$ NPs system at 400–600 nm, while the NIR localized SPR band decreases and a red shift is detected. Changes are produced due to Hg(II) ions replace Cu^+/Cu^{2+} ions forming a HgSe layer around the NPs.	A_{450}/A_{920} vs $C_{Hg(II)}$; $\Delta\lambda$ vs $C_{Hg(II)}$; A_{920} vs $C_{Hg(II)}$ (for quantification)	0–160	1.6[c]	Tap, pond, and river waters were filtered through a 0.22 μm filters. Three samples of each water were spiked with 0; 2 and 6 $\mu g\ L^{-1}$ Hg(II) ion, respectively.	39
Hg(II) inhibits the peroxidase-like activity of DNA-Ag/PtNCs on the oxidation of TMB by H_2O_2 due to the nanocluster aggregation and the decrease of Pt^{2+} surface content, resulting in the decrease of the absorption band at 652 nm.	A_{652} vs $C_{Hg(II)}$	2–40	1[c]	Samples of tap water, filtered through 0.22 μm membranes, were spiked with 4; 10; 20 and 40 $\mu g\ L^{-1}$ Hg(II) ion.	26
AuNCs catalyze the reduction of $HAuCl_4$ by H_2O_2 leading to AuNPs formation and partial aggregation. Hg(II) inhibits the catalytic activity and the AuNPs formed by residual H_2O_2 remain disperse, producing a color change. TSC accelerates the AuNPs formation.	A_{537}/A_{650} vs $C_{Hg(II)}$	0.02–2000	1.78×10^{-3}	Lake and river waters were filtered through 0.45 μm membranes. Two samples of each water were spiked with 10 and 20 $\mu g\ L^{-1}$ Hg(II).	40
Hg(II) ion produces a color change in the thiamine modified AgNPs aggregate that is spectrophotometrically measured	A_{550}/A_{395} vs $C_{Hg(II)}$	2–1000	1[c]	One river water spiked with 0; 4; 460 and 1000 $\mu g\ L^{-1}$ Hg(II) ion (standard addition method).	41
Hg(II) ion interacts with bimetallic Ag-CuNPs producing changes in the SPR absorption. As $C_{Hg(II)}$ increases, the band at 406 nm of the Ag-CuNPs absorption spectra decreases, and a second absorption peak at 504 nm is detected	A_{504}/A_{406} vs $C_{Hg(II)}$ (Milli-Q, Mengxi lake); A_{534}/A_{404} vs $C_{Hg(II)}$ (Chagan lake)	0.2–2	0.10[c]; 0.16[c]; 0.11[c] for Milli-Q, Mengxi, and Chagan waters	Lake waters were filtered through 0.22 μm membranes. Five samples of each lake were spiked with Hg(II) ion in the range 0.2 to 2 $\mu g\ L^{-1}$	42
Hg(II) ion interacts with AuNPs encapsulated in porous wood membrane forming a gold amalgam. This system catalyzes the reduction of MB by $NaBH_4$ and a decrease of the MB absorption peak is observed as $C_{Hg(II)}$ increases.	A_{662} vs $C_{Hg(II)}$	0–2	6.4×10^{-3}	Tap, deionized, and river waters. Three samples of each water spiked with 0.6; 1.2 and 1.8 $\mu g\ L^{-1}$ Hg(II) ion, respectively.	43
Hg(II) ion inhibits the peroxidase-like activity of CuO/Pt nanoflowers on the oxidation of TMB by H_2O_2 due to the CuO/Pt–Hg trimetallic amalgam formation, resulting in a decrease of the absorption at 650 nm.	A_{650} vs $C_{Hg(II)}$	0.02–140	$(9.8 \times 10^{-3})^c$ LOQ 0.024 $\mu g\ L^{-1}$ (gw)	Groundwater samples (filtered through 0.45 μm syringe filters) were spiked with 20; 30; 40; 50; 60; 70; 80; 90; 100; 110 and 120 $\mu g\ L^{-1}$ Hg(II) ion. CVASS was also applied.	27
Hg(II) ion interacts with Pzl through sulfur and nitrogen groups avoiding the aggregation of AuNPs, leading to both a decrease and an increase of absorbances at 680 and 520 nm, respectively.	$\Delta A_{680}/A_{520}$ vs $C_{Hg(II)}$	2–300	1.54[c]	Five tap and five river waters (filtered with paper) spiked with 10; 80; 160; 200 and 240 $\mu g\ L^{-1}$ Hg(II) ion. ICP-MS was also applied.	44
The T-Hg^{2+}–T complex formed by interaction of Hg with ssDNA oligonucleotide avoids the adsorption of free oligonucleotide on graphene oxide/AuNPs nanocomposite, preserving catalytic activity in the oxidation of TMB by H_2O_2.	A_{655} vs $C_{Hg(II)}$	1.04–24	0.076	Three tap and three lake waters (previously dechlorinated by boiling) were spiked with 1.8; 12 and 60 $\mu g\ L^{-1}$ Hg(II) ion. Three river waters were previously digested. Found values (verified by CVAAS) were: 0; 1.27 and 1.61 $\mu g\ L^{-1}$.	28

https://doi.org/10.1021/acsomega.2c05215
ACS Omega 2022, 7, 39574–39585

Table 1. continued

probe/sensor fundamentals	calibration graph[a]	LR (μg L^{-1})	LOD (μg L^{-1})	samples/evaluated $C_{Hg(II)}$	ref
SnTeNBs were grafted with AuNPs to form a SnTe/Au hybrid, resulting in depression of the oxidase-like activity, which is then recovered in the presence of Hg(II) due to a gold amalgam formation. Chloride ions are also determined, but [Cl$^-$] > 3 mM (e.g., seawater) interferes in the Hg(II) determination.	A_{652} vs $C_{Hg(II)}$	40−11600	30	One tap water was spiked with 0; 1200; 2400; 5000; 7000 and 9000 μg L^{-1} Hg(II) ion.	29
DNA_{mb} is immobilized on an optical fiber surface forming a stem-loop structure. In the presence of Hg(II) ion and DNA_a, the T-Hg^{2+}−T complex formation opens the stem helix in DNA_{mb} allowing the binding of its terminal end with DNA_c conjugated to AuNPs (AuNP-DNA_c), producing nanoplasmonic absorption	$(I_0-I_S)/I_0$ vs log $C_{Hg(II)}$[d]	1 × 10^{-5}-0.2	(8.76 × 10^{-7})[c]	Two drinking and two tap waters were spiked with 0.02 and 0.2 μg L^{-1} Hg(II) ion.	45
Hg(II) ion induces aggregation of AuNPs modified with two peptides, generating SPR absorption and color change	A_{720}/A_{530} vs $C_{Hg(II)}$	20−160	5.6	Lake waters, filtered through 0.45 μm membranes, were spiked with 60; 80 and 100 μg L^{-1} Hg(II) ion	46
Hg(II) ion produces a shift in the SPR wavelength of a sensing Au film due to the formation of a sandwich structure (Au/T-Hg^{2+}-T/Au) between T-modified AuNPs and T immobilized on the Au film surface of a fiber-optic	SPR shift vs $C_{Hg(II)}$	16−40	2[c]	Tap waters were spiked with 16, 20, and 40 μg L^{-1} Hg(II) ion	47

[a]Subscripts for *A* and CCT are the wavelengths in nm. $\Delta\lambda$ is the wavelength shift. [b]Wavelength difference of the first derivative of the absorption spectrum. [c]LOD = 3S_b/*m*, where S_b is the standard deviation of the blank signal and *m* is the slope of calibration line. [d]I_0 and I_S are the transmitted light intensity of the sensor in a blank and in a sample containing Hg(II) ion, respectively. *Abbreviations: A*, absorption; AFS, atomic fluorescence spectrometry; AgNPs, silver nanoparticles; AgNPRs, silver nanoprisms; AuNCs, gold nanoclusters; AuNPs, gold nanoparticles; AuNRs, gold nanorods; $C_{Hg(II)}$, concentration of Hg(II) ion; CCT, color-change time; CVAAS, cold vapor atomic absorption spectrometry; dw, distilled water; DNA_a, free assisting oligodeoxyribonucleotide probe; DNA_{mb}, oligodeoxyribonucleotide probe as a molecular beacon; DNA_r, reporting oligodeoxyribonucleotide probe; DRS diffuse reflectance spectroscopy; gw; groundwater; ICP-MS, inductively coupled plasma mass spectrometry; LOD, limit of detection; LOQ, limit of quantitation; MB, methylene blue; $NaBH_4$, sodium borohydride; NCs, nanoclusters; NIR, near-infrared; 4-NP, 4-nitrophenol; NP, nanoparticle; SnTeNBs, tin telluride nanobelts; ssDNA, single-stranded DNA; Pzl, 3,5-dimethyl-1-thiocarboxamidepyrazole; SPR, surface plasmon resonance; T, thymine; tw, tap water; TMB, 3,3′,5,5′-tetramethylbenzidine; TSC, trisodium citrate.

This approach allowed determining the original Hg(II) ion levels in real water samples (verified by atomic absorption spectroscopy) and obtaining good recoveries at the low concentrations added to the studied matrices (1 and 2 μg L^{-1}).

Two additional reports fulfilled the requirements of achieving an appropriate LOD (<2 μg L^{-1}), demonstrating a successful application to both spiked and real samples without externally added analyte and comparing the results with those provided by a reference method, but the methods were applied to too few samples (i.e., three or less).[24,32]

Another group includes the development of 15 sensors with adequate LODs but which were only applied to spiked samples, with five of them tested on very few samples. Although real matrices are preferable to synthetic ones for recovery assays, the validation of a new method should be completed by demonstrating its usefulness in real samples with no external addition of the analyte. Depending on the analytes and/or the investigated matrices, it may not be easy to obtain real samples. Despite this drawback, the authors should make an effort to include them in their working protocols and statistically compare the results with those given by a reference method. In any case, if only spiked samples are included in the analysis, at least 10 different water samples with the addition of various analyte levels are required. This would increase the analytical quality of the newly proposed methods and show that the required standards have been fully achieved.

More worrying are the 17 papers where the sensor was employed to determine mercury in samples spiked with unreasonably high analyte concentrations, even when they display LODs which apparently allowed to measure mercury levels below the official maximum. In addition, four of these latter reports studied either one or two spiked samples.

Finally, Tables 1−4 show six methods with limited applicability for the determination of mercury ion in drinking water, since they present LODs close to or higher than the target concentration of the metal ion in this type of samples. In addition, these sensors were tested on spiked samples with high concentrations of Hg(II).

An issue not considered in Tables 1−4 but of analytical relevance is the evaluation of the method selectivity. Although the chemical sensors are described as having high selectivity toward the analyte under investigation, their behavior in the presence of potential interferents must be reliably demonstrated. The most common interferents for metal ion sensors are other cations that may respond similarly to the analyte by interacting with the sensing unit. Nevertheless, it is also important to analyze the effect of certain anions that may react with the cation producing stable species, seriously affecting the analyte detection. In the specific case of the Hg(II) ion, the presence of chloride should be taken into account. In this regard, all reports shown in Tables 1−4 studied the selectivity by analyzing the effect of potentially interfering cations on the sensor signal. However, not all of them analyzed the influence of the anions. In one study, chloride was removed dechlorinating the water sample by previous boiling.[28] In other cases, the fact that this anion does not interfere was indirectly demonstrated either by using chloride salts to prepare the solutions of the investigated cations or by employing $HgCl_2$ as mercuric reagent.

5. FINAL RECOMMENDATIONS

In this section we provide some general recommendations for the development of methods for the determination of

https://doi.org/10.1021/acsomega.2c05215
ACS Omega 2022, 7, 39574−39585

Table 2. Hg(II) Ion Determination in Water Samples by Using Fluorimetric Signals

probe/sensor fundamentals	calibration graph[a]	LR ($\mu g\ L^{-1}$)	LOD ($\mu g\ L^{-1}$)	samples/evaluated $C_{Hg(II)}$	ref
AuNPs modified with thioglycolic acid quench the rhodamine B fluorescence, and the signal is restored in the presence of Hg(II) ion.	F_{581} vs $C_{Hg(II)}$	0.2−6.2	0.08[b]	One tap, one pond, and two river samples were filtered through paper. Tap and pond waters were spiked with 1 $\mu g\ L^{-1}$ Hg(II), and river samples with 2 $\mu g\ L^{-1}$ Hg(II). Original found $C_{Hg(II)}$ (verified by AAS) were 0.44 and 1.1 $\mu g\ L^{-1}$ (tap and pond waters, respectively), and 12.2 and 10.9 $\mu g\ L^{-1}$ (river samples).	31
Hg(II) ion displaces RBITC from the surface of RBITC-PEG-modified AuNPs resulting in an enhancement of RBITC fluorescence initially quenched by AuNPs.	F/F_o vs $C_{Hg(II)}$	2−100	0.46 (pure water)[b] 0.76 (river water)[b]	River water samples, filtered through 0.22 μm membranes, were spiked with 0; 2; 4; 8; 16; 30 and 60 $\mu g\ L^{-1}$ Hg(II) ion.	48
Nonfluorescent system formed by FAM-labeled ssDNA probe bound to another ssDNA probe adsorbed on WS_2 nanosheets shows fluorescence in the presence of Hg(II) ion. FAM-labeled ssDNA probe and the other oligonucleotide probe hybridize through the T-Hg^{2+}-T complex and is digested by T7 exonuclease, forming short FAM-oligonucleotide fluorescent fragments that are not adsorbed by the nanosheets.	F vs $C_{Hg(II)}$	0.1−4	0.02[b]	Tap and lake waters. Two samples of each water type were spiked with 0.4 and 2 $\mu g\ L^{-1}$ Hg(II) ion (standard addition method).	49
Hg(II) ion replaces Mn(II) ion in the surface of nonemissive Mn-doped ZnSe QDs with small size (2.1 nm), and fluorescence is detected around 600 nm.	F_{600} vs $C_{Hg(II)}$	0−900	1.4[b]	Tap and lake waters were filtered with a 0.22 μm syringe filters. Four samples of each water type were spiked with 20; 100; 400 and 800 $\mu g\ L^{-1}$ Hg(II) ion. ICP-AES was also applied.	50
Hg(II) ion quenches the fluorescence of L-cysteine-modified AuNPs. The fluorescence peak at 625 nm decreases as $C_{Hg(II)}$ increases.	F_{625} vs log $C_{Hg(II)}$	0.4−6000	0.26[b]	One tap and one river water samples, filtered through a membrane, were spiked with 1; 2 and 4 $\mu g\ L^{-1}$ Hg(II) ion (standard addition method). Original found $C_{Hg(II)}$ (verified by AFS) were 0.99 and 2.40 $\mu g\ L^{-1}$.	32
Nanocomposites formed by AgNP and reduced graphene oxide quench the rhodamine B fluorescence, and the signal is restored in the presence of Hg(II) ion.	F/F_0 vs $C_{Hg(II)}$	2.5−40	0.4[c]	Mineral, tap, and pond waters. Two samples of each water type were spiked with 10 and 20 $\mu g\ L^{-1}$ of Hg(II) ion.	51
The fluorescence of CDs@Eu-MOFs suspension at 430 nm decreases with the increasing of Hg(II) ion concentration, while at 614 nm the signal is almost constant.	F_{430}/F_{614} vs $C_{Hg(II)}$	0−60,000	0.024[c] Lowest $C_{Hg(II)} \cong$ 2000 $\mu g\ L^{-1}$	Three tap and three river water samples, filtered through a 0.22 μm filters, were spiked 1000; 2000 and 3000 $\mu g\ L^{-1}$ Hg(II) ion.	52
Hg(II) ion quenches the fluorescence of nanocrystals formed by cesium, lead, bromide perovskite and methoxypolyethylene glycol/silica composite ($CsPbBr_3$-mPEG@SiO_2). Then, the fluorescence is restored through the interaction between Hg(II) ion and GSH. Fluorescent probe can also be used for GSH detection.	F_0-F_{520}/F_0 vs $C_{Hg(II)}$	0.02−10	0.016	Tap water samples spiked with 2, 4, and 8 $\mu g\ L^{-1}$ of Hg(II) ion.	53
Hg(II) ion interacts with a biosensor integrated with a selected FNA with T-rich DNA sequence and, due to the T-Hg^{2+}−T complex formation and through FRET mechanism, the fluorescence signal is increased. Pb(II) ion is simultaneously detected using RNA-cleaving Pb^{2+}-specific DNAzyme as FNA.	F vs $C_{Hg(II)}$ The first part of sigmoidal plot is used for calibration.	0−30	0.844[b]	No pretreatment needed for tap, bottled, lake, and underground waters. Three samples of each type of water were spiked with 30; 52 and 90 $\mu g\ L^{-1}$ Hg(II) ion. ICP-AES was also applied.	54
LYSO-QF probe forms tetrameric, trimeric, and dimeric complexes at different $C_{Hg(II)}$ ranges giving three fluorescent emission ranges depending on the Hg(II) concentration.	F_{495} vs $C_{Hg(II)}$ (signal ↓); F_{512} vs $C_{Hg(II)}$ (signal ↑); F_{694} vs $C_{Hg(II)}$ (signal ↑)	0−600; 1400−2300; 2800−4100	2.2[b] (F_{495} vs $C_{Hg(II)}$ was used). Lowest $C_{Hg(II)} \cong$ 100 $\mu g\ L^{-1}$	Two samples of each water (tap, pond, and river waters) were spiked with 2 and 5 $\mu g\ L^{-1}$ Hg(II) ion. AAS was also applied.	55

[a]Subscript for F is the emission wavelength in nm. [b]LOD = $3S_b/m$, where S_b is the standard deviation of the blank signal and m is the slope of calibration line. [c]LOD = $3S_I/m$, where S_I is the standard deviation of the intercept and m is the slope of calibration line. Abbreviations: AAS, atomic absorption spectroscopy; AFS, atomic fluorescence spectrometry; AgNPs, silver nanoparticles; AuNPs, gold nanoparticles; $C_{Hg(II)}$, concentration of Hg(II) ion; CDs@Eu-MOFs, carbon dots-embedded europium metal−organic frameworks; F, fluorescence intensity; FAM, fluorescein amidite; FNA, functional nucleic acid; FRET, fluorescence resonance energy transfer; GSH, glutathione; ICP-AES, inductively coupled plasma-atomic emission spectrometry; LOD, limit of detection; LR, linear range; LYSO-QF, (Z)-N-((Z)-2-(1,3,3-trimethylindolin-2ylidene)ethylidene)quinoline-8-amine; NP, nanoparticle; PEG, poly(ethylene glycol); QDs, quantum dots; ssDNA, single-stranded DNA; RBITC, rhodamine B isothiocyanate; T, thymine; WS_2, tungsten disulfide.

https://doi.org/10.1021/acsomega.2c05215
ACS Omega 2022, 7, 39574−39585

Table 3. Hg(II) Ion Determination in Water Samples by Using Surface-Enhanced Raman Scattering Signal

probe/sensor fundamentals	calibration graph[a]	LR (μg L^{-1})	LOD (μg L^{-1})	samples/evaluated $C_{Hg(II)}$	ref
Through the strong mercury and sulfur bond, Hg(II) ion prevents the adsorption of MESNA on the surface of AgNPs resulting in a decrease of SERS of the MESNA modified AgNPs.	ΔI_{795} vs $C_{Hg(II)}$	2−400	0.48[b]	Water samples of two different lakes and groundwater samples were spiked with 40 and 240 μg L^{-1} Hg(II) ion.	56
Hg(II) ion interacts with IP_6 stabilized AuNPs modified by CV and TC, decreasing the intensity of SERS band of the probe at 1173 cm^{-1} due to the CV molecules detachment from the surface.	I_{1173}/I_0 vs $C_{Hg(II)}$	0.1−1	1×10^{-4}	Five tap and five river water samples were spiked with 0.4 μg L^{-1} Hg(II) ion.	57
Hg(II) ion changes the SERS signal of DNA modified AuNPs and 4-nitrothiophenol system, through the transformation of ssDNA into double helical DNA by T−Hg^{2+}−T interaction. Au nanochains length grew longer with increasing the $C_{Hg(II)}$ ion, and the increase of SERS signal is detected.	I_{1344} vs $C_{Hg(II)}$	0.001−0.5	(4.5×10^{-4})[b]	Three drinking water samples were spiked with 0.04; 0.08 and 0.15 μg L^{-1} Hg(II) ion.	58
Nanostructured gold substrate functionalized with a crown ether formed by ADB18C6 and MPA as SERS reporter is employed. The binding of Hg(II) ion into the crown ether layer cavity increases the intensity of Raman band at 1501 cm^{-1}.	I_{1501} vs log $C_{Hg(II)}$	0.002−200	(1.02×10^{-4})[b]	One tap water sample was spiked with 5 μg L^{-1} Hg(II) ion.	59
Surface modified AuNRAs with 4-MPBA as SERS reporter are employed. In the presence of Hg(II) ion spectral changes of reporter including the disappearance, emergence, and shift of Raman peaks are detected.	log I vs −log $C_{Hg(II)}$ I measured at 467, 1048, 1085, and 1536 cm^{-1}	0.02−2000	ca. 0.02 by visual inspection	One lake water sample and one groundwater sample, each spiked with 2 μg L^{-1} Hg(II) ion. AFS was applied for results comparison.	60
Hg(II) ion interacts with surface-stabilized HEPES-AuNSs on a paper substrate forming a AuHg amalgam. The substrate is incubated in a $HAuCl_4$, HCl and H_2O_2 solution with 4-MBA (reporter). SERS bands decrease as the $C_{Hg(II)}$ increases.	peak area (1590) vs −log $C_{Hg(II)}$	0.02−200	0.006[b] 0.066 (seawater)[b] 0.046 (pond water)[b]	Three seawater samples and three pond water samples, each spiked with 0.2; 2 and 20 μg L^{-1} Hg(II) ion.	61
A chip formed by AuNPs immobilized on aminopropyl trimethoxysilane modified ITO surface and assembled GSH molecules was constructed, and 4-Mpy was used as SERS reporter. The interaction of Hg(II) ion with the chip GSH molecules and 4-Mpy increases the intensity of SERS peaks of 4-Mpy. $C_{Hg(II)}$ is measured through the 1093 cm^{-1} band intensity.	$\Delta I_{1093\ cm^{-1}}$ vs −log $C_{Hg(II)}$	0.002−200	1.76×10^{-3}	Five seawater samples were filtered through filter paper and 0.22 μm microporous filters. Samples were spiked with 0; 0.002; 0.02; 0.2 and 2 μg L^{-1} Hg(II) ion. Samples with 0.2 and 2 μg L^{-1} Hg(II) also were investigated with ICP-MS.	62

[a]Subscript for I is the wavelength in cm^{-1}. [b]LOD = $3S_b/m$, where S_b is the standard deviation of the blank signal and m is the slope of calibration line. Abbreviations: A, absorbance; ADB18C6, aminodibenzo-18-crown-6 derivative; AFS, atomic fluorescence spectrometry; AgNPs, silver nanoparticles; AuNPs, gold nanoparticles; AuNRAs, Au nanorod arrays; AuNSs, gold nanostars; $C_{Hg(II)}$, concentration of Hg(II) ion; CV, violet crystal; GSH, glutathione; HEPES, 2-[4-(2-hydroxyethel) piperazine-1-yl]ethanesulfonic acid; I, intensity; ICP−MS, inductively coupled plasma mass spectrometry; IP_6, inositol hexaphosphate; ITO, indium tin oxide; LOD, limit of detection; LR, linear range; MPA, mercaptopropionic acid; 4-MBA, 4-mercaptobenzonic acid; MESNA, sodium 2-mercaptoethanesulfonate; 4-MPBA, 4-mercaptophenylboronic acid; 4-Mpy, 4-mercaptopyridine; NIR, near-infrared; NPs, nanoparticles; SERS, surface-enhanced Raman scattering; ssDNA, single-stranded DNA; T, thymine; TC, trisodium citrate; TMB, 3,3′,5,5′-tetramethylbenzidine.

https://doi.org/10.1021/acsomega.2c05215
ACS Omega 2022, 7, 39574−39585

Table 4. Hg(II) Ion Determination in Water Samples by Using Dual Spectroscopic Signals

probe/sensor fundamentals	calibration graph[a]	LR (μg L^{-1})	LOD (μg L^{-1})	samples/evaluated $C_{Hg(II)}$	ref
Fluorimetric/Absorptimetric Modes of Detection					
Hg(II) ion inhibits the PtNPs catalytic activity on OPD oxidation with H_2O_2 due to a Pt−Hg amalgam formation in the NP surface. Both the fluorescence intensity and the yellow color of the system decrease as the $C_{Hg(II)}$ increase.	F_{555} vs $C_{Hg(II)}$	2−400 (Flu)	0.028[b] (Flu)	Two river water samples were centrifuged and filtered through 0.45 μm membranes, and then they were spiked with 10 and 20 μg L^{-1} Hg(II) ion.	63
	A_{420} vs $C_{Hg(II)}$	2−400(Abs)	0.16[b] (Abs)		
Hg(II) ion produces both fluorescence enhancement and peroxidase-like activity decrease of FAM-labeled Hg^{2+} aptamer adsorbed on P-CeO_2NRs. The T-Hg^{2+}−T complex formation induces the separation of FAM-apt from the NRs surface, resulting in the recovery of FAM-apt fluorescence. The peroxidase-like activity of P-CeO_2 NRs decreases and the color of TMB-H_2O_2 solution turned to light blue.	F_{520} vs log $C_{Hg(II)}$	0.016−2.5 (Flu)	0.0158[b] (Flu)	Canal waters were filtered through 0.22 μm membranes. Two samples were spiked with 0.6 and 2 μg L^{-1} Hg(II) ion (Flu and Abs); one sample was spiked with 0.06 μg L^{-1} Hg(II) ion (Flu); and one sample was spiked with 6 μg L^{-1} Hg(II) ion (Abs).	64
	A_{650} vs log $C_{Hg(II)}$	0.1−20(Abs)	0.062[b] (Abs)		
Absorptimetric/SERS Modes of Detection					
Hg(II) ion reverses the Bismuthiol II-induced aggregation of AuNPs, resulting in both UV−vis and SERS spectral changes.	A_{780}/A_{530} vs $C_{Hg(II)}$	0−30(Abs)	0.4[b](Abs)	One tap and one spring water samples were each spiked with 18 μg L^{-1} Hg(II) ion (Abs). CVAFS was also applied.	65
	I_{1364} vs $C_{Hg(II)}$	0−30 (SERS)	6[b] (SERS)		
Hg(II) ion inhibits the oxidation of TMB by H_2O_2 catalyzed by Au core AgPt shell NPs modified with mercaptohexanol. As $C_{Hg(II)}$ increases, the generation of the oxidized form of TMB (oxTMB) decreases, resulting in both a color change of the system and a decrease in the intensities of the SERS bands of oxTMB.	A_{652} vs log $C_{Hg(II)}$	200−20,000 (Abs)	104[b] (Abs)	Six ultrapure waters were spiked with 0.4; 4 and 40 μg L^{-1} Hg(II) ion (SERS), and 1600; 4000 and 16 000 μg L^{-1} Hg(II) ion (Abs). Five filtered river waters were spiked with 0.4; 4 and 40 μg L^{-1} Hg(II) ion (SERS), and 1,600 and 16,000 μg L^{-1} Hg(II) ion (Abs).	66
	I_{1608} vs log $C_{Hg(II)}$	0.2−2000 (SERS)	0.056[b] (SERS)		
Hg(II) ion suppress the etching effect of $S_2O_3^{2-}$ on silver shells of Ag-coated AuNPs due to the HgS formation. Both the absorption at 394 nm and the Raman intensity of R6G increases as the $C_{Hg(II)}$ increase.	ΔA_{394} vs $C_{Hg(II)}$	200−1000 (Abs)	40 (Abs)	One tap water sample was spiked with 400 μg L^{-1} Hg(II) ion (Abs), and with 2 μg L^{-1} Hg(II) ion (SERS). One lake water sample, filtered through a 0.22 μm membrane, was spiked with 400 μg L^{-1} Hg(II) ion (Abs), and with 2 μg L^{-1} Hg(II) ion (SERS).	67
	ΔI_{1362} vs − log $C_{Hg(II)}$	0.02−200 (SERS)	0.02 (SERS)		

[a]Subscripts for F and A indicate the wavelength in nm, those for I the wavenumber in cm^{-1}. [b]LOD = $3S_b/m$, where S_b is the standard deviation of the blank signal and m is the slope of calibration line. Abbreviations: A, absorbance; Abs, absorptimetric approach; AuNPs, gold nanoparticles; Bismuthiol II, potassium 5-mercapto-3-phenyl-1,3,4-thiadiazole-2-thione; $C_{Hg(II)}$, concentration of Hg(II) ion; CVAFS, cold vapor atomic fluorescence spectrometry; F, fluorescence intensity; FAM, carboxyfluorescein; Flu, fluorimetric approach; LOD, limit of detection; LR, linear range; NPs, nanoparticles; OPD, o-phenylenediamine; P-CeO_2NRs, porous cerium oxide nanorods; PtNPs, platinum nanoparticles; R6G, rhodamine 6G; SERS, surface-enhanced Raman scattering; TMB, 3,3′,5,5′-tetramethylbenzidine.

https://doi.org/10.1021/acsomega.2c05215
ACS Omega 2022, 7, 39574−39585

inorganic species in drinking water, using Hg(II) as an example. Most scientific reports on the development of sensing platforms for Hg(II) allocate ca. 90% of the space to the detailed description of the synthesis, preparation, structural study, physicochemical characterization, etc., while the analytical sections are usually very brief. We suggest to expand the latter section following some standard rules for analytical calibration and validation.

A first phase of any protocol attempting to develop a methodology for detecting Hg(II) in drinking water is to roughly estimate the LOD. If this latter value is above 2 $\mu g\ L^{-1}$, this means that a preconcentration procedure is required.

Once the detectability of the method has been found to be feasible, the following steps should be followed:

1. Prepare and measure a set of calibration standards from 0.1 to 0.2 $\mu g\ L^{-1}$ to ca. 50−100 $\mu g\ L^{-1}$.
2. If the calibration graph is linear, use the IUPAC test for setting the maximum concentration at which linearity is complied. Do not rely on the correlation coefficient.
3. Estimate the LOD using the modern IUPAC definition.
4. Analyze at least 10 spiked water samples, with final concentrations of Hg in the range 0.5 to 5 $\mu g\ L^{-1}$. Compare the estimated value of the added concentrations with the nominal ones using a statistical test.
5. Analyze at least 10 real, unspiked drinking water samples and compare the results with a reference method, i.e., atomic spectrometry. Use suitable statistical tests for the comparison.

CONCLUSION

In view of the above discussion and findings, the conclusions of the present report are rather disappointing. The proposal of new sensors for measuring the concentrations of heavy metal ions in drinking water, particularly in the case of the highly toxic mercury ions, demands authors to comply with a series of requirements for proper method development, validation, and applicability study. These are not met in the vast majority of the reviewed publications, with only a very small number of reports employing the correct analytical standards.

The authors of the present review would like to call the attention of reviewers and editors of international journals on the importance of verifying that submitted manuscripts describing spectroscopic sensors for the determination of low concentration species, from heavy metal ions to all potential organic contaminants, meet modern analytical standards. Otherwise, the usefulness of the proposed sensors would be highly limited.

AUTHOR INFORMATION

Corresponding Authors

Alejandro C. Olivieri − *Departamento de Química Analítica, Facultad de Ciencias Bioquímicas y Farmacéuticas, Universidad Nacional de Rosario, Instituto de Química Rosario (CONICET-UNR), 2000 Rosario, Argentina;* orcid.org/0000-0003-4276-0369; Email: olivieri@iquir-conicet.gov.ar

Graciela M. Escandar − *Departamento de Química Analítica, Facultad de Ciencias Bioquímicas y Farmacéuticas, Universidad Nacional de Rosario, Instituto de Química Rosario (CONICET-UNR), 2000 Rosario, Argentina;* orcid.org/0000-0001-8308-6433; Email: escandar@iquir-conicet.gov.ar

Complete contact information is available at: https://pubs.acs.org/10.1021/acsomega.2c05215

Notes

The authors declare no competing financial interest.

ACKNOWLEDGMENTS

The authors are grateful to UNR (Universidad Nacional de Rosario), CONICET (Consejo Nacional de Investigaciones Científicas y Técnicas) and ANPCyT (Agencia Nacional de Promoción Científica y Tecnológica, project PICT 2020-00179) for financial support.

REFERENCES

(1) WHO (World Health Organization). *Guidelines for Drinking-water Quality*, 4th ed.; World Health Organization: Geneva, 2011.

(2) U.S. Environmental Protection Agency (USEPA). Regulated drinking water contaminants (2015). https://www.epa.gov/sites/default/files/2015-10/documents/ace3_drinking_water.pdf.

(3) Chowdhury, S.; Mazumder, M.A. J.; Al-Attas, O.; Husain, T. Heavy metals in drinking water: Occurrences, implications, and future needs in developing countries. *Sci. Total Environ.* **2016**, *569−570*, 476−488.

(4) Kallithrakas-Kontos, N.; Foteinis, S. Recent advances in the analysis of mercury in water − Review. *Curr. Anal. Chem.* **2015**, *12*, 22−36.

(5) U.S. Environmental Protection Agency (USEPA). National primary drinking water regulations. Inorganic Chemicals. https://www.epa.gov/ground-water-and-drinking-water/national-primary-drinking-water-regulations#Inorganic (accessed August 2022).

(6) Bernhoft, R. A. Mercury toxicity and treatment: A review of the literature. *J. Environ. Public Health* **2012**, *2012*, 460508.

(7) U.S. Environmental Protection Agency (USEPA). *Method 245.1: Determination of mercury in water by cold vapor atomic absorption spectrometry. Revision 3.0*. USEPA: Cincinnati, OH, 1994.

(8) Olivieri, A. C. Practical guidelines for reporting results in single- and multi-component analytical calibration: A tutorial. *Anal. Chim. Acta* **2015**, *868*, 10−22.

(9) Currie, L. A. Nomenclature in evaluation of analytical methods including quantification and detection capabilities. *Pure Appl. Chem.* **1995**, *67*, 1699−1723.

(10) Skogerboe, R. K.; Grant, C. L. Comments on the definitions of the terms sensitivity and detection limit. *Spectrosc. Lett.* **1970**, *3*, 215−220.

(11) Cuadros Rodríguez, L.; García Campaña, A. M.; Jiménez Linares, C.; Román Ceba, M. Estimation of performance characteristics of an analytical method using the data set of the calibration experiment. *Anal. Lett.* **1993**, *26*, 1243−1258.

(12) Danzer, K.; Currie, L. A. Guidelines for calibration in analytical chemistry. Part 1. Fundamentals and single component calibration. *Pure Appl. Chem.* **1998**, *70*, 993−1014.

(13) Raposo, F. Evaluation of analytical calibration based on least-squares linear regression for instrumental techniques: A tutorial review. *Trends Anal. Chem.* **2016**, *77*, 167−185.

(14) Currie, L. A. Limits for qualitative detection and quantitative determination. Application to radiochemistry. *Anal. Chem.* **1968**, *40*, 586−593.

(15) Hubaux, A.; Vos, G. Decision and detection limits for calibration curves. *Anal. Chem.* **1970**, *42*, 849−855.

(16) Currie, L. A. Nomenclature in evaluation of analytical methods, including quantification and detection capabilities. *Pure Appl. Chem.* **1995**, *67*, 1699−1723.

(17) ISO 11843. Capability of detection. International Standards Organisation, Geneva. https://www.iso.org/obp/ui/#iso:std:iso:11843:-1:ed-1:en.

(18) Dillingham, P. W.; Alsaedi, B. S. O.; Granados-Focil, S.; Radu, A.; McGraw, C. M. Establishing meaningful limits of detection for

ion-selective electrodes and other nonlinear sensors. *ACS Sens.* **2020**, *5*, 250−257.
(19) Miller, J. N.; Miller, J. C.*Statistics and chemometrics for analytical chemistry*, 4th ed.; Prentice-Hall: Harlow, UK, 2000.
(20) González, A. G.; Herrador, M. A. A practical guide to analytical method validation, including measurement uncertainty and accuracy profiles. *Trends Anal. Chem.* **2007**, *26*, 227−238.
(21) van der Voet, H. Comparing the predictive accuracy of models using a simple randomization test. *Chemom. Intell. Lab. Syst.* **1994**, *25*, 313−323.
(22) Du, J.; Jiang, L.; Shao, Q.; Liu, X.; Marks, R. S.; Ma, J.; Chen, X. Colorimetric detection of mercury ions based on plasmonic nanoparticles. *Small* **2013**, *9*, 1467−1481.
(23) Pomal, N. C.; Bhatt, K. D.; Modi, K. M.; Desai, A. L.; Patel, N. P.; Kongor, A.; Kolivoška, V. Functionalized silver nanoparticles as colorimetric and fluorimetric sensor for environmentally toxic mercury ions: an overview. *J. Fluoresc.* **2021**, *31*, 635−649.
(24) Tao, H.; Lin, Y.; Yan, L.; Di, J. A plasmonic mercury sensor based on silver−gold alloy nanoparticles electrodeposited on indium tin oxide glass. *Electrochem. Commun.* **2014**, *40*, 75−79.
(25) Morris, T.; Copeland, H.; McLinden, E.; Wilson, S.; Szulczewski, G. The effects of mercury adsorption on the optical response of size-selected gold and silver nanoparticles. *Langmuir* **2002**, *18*, 7261−7264.
(26) Wu, L. L.; Wang, L. Y.; Xie, Z. J.; Xue, F.; Peng, C. F. Colorimetric detection of Hg2+ based on inhibiting the peroxidase-like activity of DNA-Ag/Pt nanoclusters. *RSC Adv.* **2016**, *6*, 75384−75389.
(27) Lian, Q.; Liu, H.; Zheng, X.; Li, X.; Zhang, F.; Gao, J. Enhanced peroxidase-like activity of CuO/Pt nanoflowers for colorimetric and ultrasensitive Hg2+ detection in water sample. *Appl. Surf. Sci.* **2019**, *483*, 551−561.
(28) Qi, Y.; Song, D.; Chen, Y. Colorimetric oligonucleotide-based sensor for ultra-low Hg2+ in contaminated environmental medium: convenience, sensitivity and mechanism. *Sci. Total Environ.* **2021**, *766*, 142579.
(29) Zhang, M.; Qu, Y.; Li, D.; Liu, X.; Niu, Y.; Xu, Y. To love and to kill: accurate and selective colorimetry for both chloride and mercury ions regulated by electro-synthesized oxidase-like SnTe nanobelts. *Anal. Chem.* **2021**, *93*, 10132−10140.
(30) Sun, Z.; Du, J.; Jing, C. Recent progress in detection of mercury using surface enhanced Raman spectroscopy - A review. *J. Environm. Sci.* **2016**, *39*, 134−143.
(31) Zheng, A.; Chen, J.; Wu, G.; Wei, H.; He, C.; Kai, X.; Wu, G.; Chen, Y. Optimization of a sensitive method for the "switch-on" determination of mercury(II) in waters using Rhodamine B capped gold nanoparticles as a fluorescence sensor. *Microchim. Acta* **2009**, *164*, 17−27.
(32) Ma, X.; Wang, Z.; He, S.; Zhao, J.; Lai, X.; Xu, J. L-Cysteine modified gold nanoparticles for tube-based fluorometric determination of mercury (II) ions. *Microchim. Acta* **2019**, *186*, 1−8.
(33) Rex, M.; Hernandez, F. E.; Campiglia, A. D. Pushing the limits of mercury sensors with gold nanorods. *Anal. Chem.* **2006**, *78*, 445−451.
(34) Yin, C.; Iqbal, J.; Hu, H.; Liu, B.; Zhang, L.; Zhu, B.; Du, Y. Sensitive determination of trace mercury by UV−visible diffuse reflectance spectroscopy after complexation and membrane filtration-enrichment. *J. Hazard. Mater.* **2012**, *233*−*234*, 207−212.
(35) Chen, L.; Fu, X.; Lu, W.; Chen, L. Highly sensitive and selective colorimetric sensing of Hg2+ based on the morphology transition of silver nanoprisms. *ACS Appl. Mater. Interfaces* **2013**, *5*, 284−290.
(36) Sener, G.; Uzun, L.; Denizli, A. Lysine-promoted colorimetric response of gold nanoparticles: a simple assay for ultrasensitive mercury (II) detection. *Anal. Chem.* **2014**, *86*, 514−520.
(37) Bhattacharjee, Y.; Chakraborty, A. Label-free cysteamine-capped silver nanoparticle-based colorimetric assay for Hg(II) detection in water with subnanomolar exactitude. *ACS Sustainable Chem. Eng.* **2014**, *2*, 2149−2154.
(38) Chen, Z.; Zhang, C.; Gao, Q.; Wang, G.; Tan, L.; Liao, Q. Colorimetric signal amplification assay for mercury ions based on the catalysis of gold amalgam. *Anal. Chem.* **2015**, *87*, 10963−10968.
(39) Zhang, H.; Xia, Y. Ratiometry, wavelength, and intensity: triple signal readout for colorimetric sensing of mercury ions by plasmonic Cu2-xSe nanoparticles. *ACS Sens.* **2016**, *1*, 384−391.
(40) Zhou, Y.; Ma, Z. Colorimetric detection of Hg2+ by Au nanoparticles formed by H2O2 reduction of HAuCl4 using Au nanoclusters as the catalyst. *Sensor. Actuat. B-Chem.* **2017**, *241*, 1063−1068.
(41) Khan, U.; Niaz, A.; Shah, A.; Zaman, M. I.; Zia, M. A.; Iftikhar, F. J.; Nisar, J.; Ahmed, M. N.; Akhter, M. S.; Shah, A. H. Thiamine functionalized silver nanoparticles for the highly selective and sensitive colorimetric detection of Hg2+ ions. *New J. Chem.* **2018**, *42*, 528−534.
(42) Li, S.; Wei, T.; Tang, M.; Chai, F.; Qu, F.; Wang, C. Facile synthesis of bimetallic Ag-Cu nanoparticles for colorimetric detection of mercury ion and catalysis. *Sensor Actuat. B-Chem.* **2018**, *255*, 1471−1481.
(43) Hai, J.; Chen, F.; Su, J.; Xu, F.; Wang, B. Porous wood members-based amplified colorimetric sensor for Hg2+ detection through Hg2+-triggered methylene blue reduction reactions. *Anal. Chem.* **2018**, *90*, 4909−4915.
(44) Kataria, R.; Sethuraman, K.; Vashisht, D.; Vashisht, A.; Mehta, S. K.; Gupta, A. Colorimetric detection of mercury ions based on anti-aggregation of gold nanoparticles using 3, 5-dimethyl-1-thiocarbox-amidepyrazole. *Microchem. J.* **2019**, *148*, 299−305.
(45) Fan, S. M.; Chiang, C. Y.; Tseng, Y. T.; Wu, T. Y.; Chen, Y. L.; Huang, C. J.; Chau, L. K. Detection of Hg(II) at part-per-quadrillion levels by fiber optic plasmonic absorption using DNA hairpin and DNA-gold nanoparticle conjugates. *ACS Appl. Nano Mater.* **2021**, *4*, 10128−10135.
(46) Li, X. Y.; Zhang, M. M.; Zhou, X. D.; Hu, J. M. A functional peptide-mediated colorimetric assay for mercury ion based on dual-modified gold nanoparticles. *Anal. Biochem.* **2021**, *631*, 114369.
(47) Yuan, H.; Sun, G.; Peng, W.; Ji, W.; Chu, S.; Liu, Q.; Liang, Y. Thymine-functionalized gold nanoparticles (Au NPs) for a highly sensitive fiber-optic surface plasmon resonance mercury ion nano-sensor. *Nanomaterials* **2021**, *11*, 397.
(48) Liu, D.; Wang, S.; Swierczewska, M.; Huang, X.; Bhirde, A. A.; Sun, J.; Wang, Z.; Yang, M.; Jiang, X.; Chen, X. Highly robust, recyclable displacement assay for mercuric ions in aqueous solutions and living cells. *ACS Nano* **2012**, *6*, 10999−11008.
(49) Ge, J.; Xin-Geng; Du, Y.-H.; Chen, J.-J.; Zhang, L.; Bai, D.-M.; Ji, D.-Y.; Hu, Y.-L.; Li, Z.-H. Highly sensitive fluorescence detection of mercury (II) ions based on WS2 nanosheets and T7 exonuclease assisted cyclic enzymatic amplification. *Sensor. Actuat. B-Chem.* **2017**, *249*, 189−194.
(50) Zhou, Z. Q.; Yan, R.; Zhao, J.; Yang, L. Y.; Chen, J. L.; Hu, Y. J.; Jiang, F. L.; Liu, Y. Highly selective and sensitive detection of Hg2+ based on fluorescence enhancement of Mn-doped ZnSe QDs by Hg2+-Mn2+ replacement. *Sensor. Actuat. B-Chem.* **2018**, *254*, 8−15.
(51) Sahu, D.; Sarkar, N.; Mohapatra, P.; Swain, S. K. Rhodamine B associated Ag/r-GO nanocomposites as ultrasensitive fluorescent sensor for Hg2+. *Microchem. J.* **2020**, *154*, 104577.
(52) Guo, H.; Wang, X.; Wu, N.; Xu, M.; Wang, M.; Zhang, L.; Yang, W. In-situ synthesis of carbon dots-embedded europium metal-organic frameworks for ratiometric fluorescence detection of Hg2+ in aqueous environment. *Anal. Chim. Acta* **2021**, *1141*, 13−20.
(53) Shu, Y.; Sun, L.; Wang, Y.; Jin, D.; Xu, Q.; Hu, X. Polymer surface ligand and silica coating induced highly stable perovskite nanocrystals with enhanced aqueous fluorescence for efficient Hg2+ and glutathione detection. *Analyst* **2021**, *146*, 6798−6807.
(54) Zhou, Y.; Yi, Z.; Song, D.; Wang, H.; Zhao, S.; Long, F.; Zhu, A. Development of a two-in-one integrated bioassay for simultaneous and rapid on-site detection of Pb2+ and Hg2+ in water. *Anal. Chim. Acta* **2022**, *1194*, 339397.
(55) Muthusamy, S.; Zhao, L.; Rajalakshmi, K.; Zhu, D.; Wang, S.; Mack, J.; Lee, K. B.; Zhang, L.; Zhu, W. Quantitative Hg2+ detection

https://doi.org/10.1021/acsomega.2c05215
ACS Omega 2022, 7, 39574−39585

via forming three coordination complexes using a lysosome targeting quinoline - Fisher aldehyde fluorophore. *Talanta* **2022**, *236*, 122884.
(56) Chen, Y.; Wu, L.; Chen, Y.; Bi, N.; Zheng, X.; Qi, H.; Qin, M.; Liao, X.; Zhang, H.; Tian, Y. Determination of mercury(II) by surface-enhanced Raman scattering spectroscopy based on thiol-functionalized silver nanoparticles. *Microchim. Acta* **2012**, *177*, 341−348.
(57) Fu, S.; Guo, X.; Wang, H.; Yang, T.; Wen, Y.; Yang, H. Detection of trace mercury ions in water by a novel Raman probe. *Sensor. Actuat. B-Chem.* **2014**, *199*, 108−114.
(58) Xu, L.; Yin, H.; Ma, W.; Kuang, H.; Wang, L.; Xu, C. Ultrasensitive SERS detection of mercury based on the assembled gold nanochains. *Biosens. Bioelectron.* **2015**, *67*, 472−476.
(59) Sarfo, D. K.; Sivanesan, A.; Izake, E. L.; Ayoko, G. A. Rapid detection of mercury contamination in water by surface enhanced Raman spectroscopy. *RSC Adv.* **2017**, *7*, 21567−21575.
(60) Zhao, Q.; Zhang, H.; Fu, H.; Wei, Y.; Cai, W. Raman reporter-assisted Au nanorod arrays SERS nanoprobe for ultrasensitive detection of mercuric ion (Hg2+) with superior anti-interference performances. *J. Hazard. Mater.* **2020**, *398*, 122890.
(61) Yang, P. C.; Lin, P. H.; Huang, C. C.; Wu, T.; Lin, Y. W. Determination of Hg(II) based on the inhibited catalytic growth of surface-enhanced Raman scattering-active gold nanoparticles on a patterned hydrophobic paper substrate. *Microchem. J.* **2020**, *157*, 104983.
(62) Zheng, Q.; Teng, X.; Li, Q.; Ma, Z.; Ying, Y.; Wu, Y.; Wen, Y.; Guo, X.; Yang, H. A Raman chip for rapid and specific detection of trace mercury ions in seawater. *Sensor. Actuat. B-Chem.* **2021**, *346*, 130468.
(63) Zhou, Y.; Ma, Z. Fluorescent and colorimetric dual detection of mercury (II) by H2O2 oxidation of o-phenylenediamine using Pt nanoparticles as the catalyst. *Sensor Actuat B-Chem.* **2017**, *249*, 53−58.
(64) Li, J.; Li, L.; Bi, X.; Liu, X.; Luo, L.; You, T. Fluorescence/colorimetry dual-mode sensing strategy for mercury ion detection based on the quenching effect and nanozyme activity of porous cerium oxide nanorod. *Sensor. Actuat. B-Chem.* **2022**, *360*, 131483.
(65) Duan, J. L.; Yang, M.; Lai, Y. C.; Yuan, J. P.; Zhan, J. H. A colorimetric and surface-enhanced Raman scattering dual-signal sensor for Hg2+ based on Bismuthiol II-capped gold nanoparticles. *Anal. Chim. Acta* **2012**, *723*, 88−93.
(66) Song, C.; Li, J.; Sun, Y.; Jiang, X.; Zhang, J.; Dong, C.; Wang, L. Colorimetric/SERS dual-mode detection of mercury ion via SERS-Active peroxidase-like Au@AgPt NPs. *Sensor. Actuat. B-Chem.* **2020**, *310*, 127849.
(67) Wang, J.; Wu, J.; Zhang, Y.; Zhou, X.; Hu, Z.; Liao, X.; Sheng, B.; Yuan, K.; Wu, X.; Cai, H.; Zhou, H.; Sun, P. Colorimetric and SERS dual-mode sensing of mercury (II) based on controllable etching of Au@Ag core/shell nanoparticles. *Sensor. Actuat. B-Chem.* **2021**, *330*, 129364.

https://doi.org/10.1021/acsomega.2c05215
ACS Omega 2022, 7, 39574−39585